Journal of Nanophotonics

Nanophotonics.SPIEDigitalLibrary.org

Review of nanostructure color filters

Felix Gildas
Yaping Dan

SPIE.

Felix Gildas, Yaping Dan, "Review of nanostructure color filters," *J. Nanophoton.* **13**(2), 020901 (2019), doi: 10.1117/1.JNP.13.020901.

REVIEW

Review of nanostructure color filters

Felix Gildas and Yaping Dan*
University of Michigan–Shanghai Jiao Tong University Joint Institute, Shanghai, China

Abstract. Nanostructure color filters filter light spectrum via the structural engineering, unlike traditional dye filters that rely on the chemical compositions to absorb light. In light of the successful advance in micro/nanofabrication technology in the past decades, these structured color filters are particularly promising for future applications in ultrascaled color filtering and multispectral imaging. We will summarize the recent progress in nanostructure color filters based on plasmonics, nanowires, metamaterials, and quantum dots (QDs). Plasmonics filters rely on surface plasmon resonances to realize the spectrum selection. For nanowire color filters, the color filtering is achieved by light coupling into the leaky or waveguiding mode in nanowires. In metamaterial filters, the refractive index of artificial materials is manipulated to create a broad color palette. QDs color filters rely on bandgap engineering to create filtering effects by simply altering the size and composition of the QDs. Clearly, the above filtering technologies have their own pros and cons, which will be analyzed. © *2019 Society of Photo-Optical Instrumentation Engineers (SPIE)* [DOI: 10.1117/1.JNP.13.020901]

Keywords: color filter; nanostructure; plasmonic; nanowire; metamaterial; quantum dot.

Paper 18151V received Sep. 20, 2018; accepted for publication May 22, 2019; published online Jun. 17, 2019.

1 Introduction

Traditional color filters made of pigments and dyes are long established in complementary metal oxide semiconductor (CMOS) image sensors, organic light emitting devices (OLED), and liquid crystal displays (LCD). These color filters are based on the selective absorption of colorful lights by the filtering materials.[1] Unfortunately, the organic filtering materials are susceptible to heat and ultraviolet radiation due to their relatively low chemical stability, often resulting in degradation in filtering performances. Additionally, for a full Bayer's color, three types of pigments or dyes have to be integrated together by multistep processes.[2] The growing demand of miniaturization of electronic devices has made the multistep integration increasingly expensive and difficult. For multispectral imaging in particular, the integration process of many types of organic filtering materials becomes extremely challenging. A revolution in color filtering technology is highly needed.

Inspired by natural color filters seen in butterflies, beetles, and other species,[3–9] researchers have studied and demonstrated various structural color filters in the past decades.[10] The concept of structural color filters was actually first explored by Hooke in 1665 when he elucidated the structural color of silver fish,[11] although another study claimed that the usage of nanostructure has already begun three millennia ago.[12] Later on, scientists found that by adjusting its surface structure, it is possible to manipulate the light interaction with the object via scattering, reflection, and diffraction or a mix of them, creating colors visible to observers. This discovery led to the ever-growing field of structural color filters based on metal surface plasmonics,[13] nanowire waveguides,[14] metamaterials,[15] and even quantum dots (QDs).[16] The improvement of electron microscopy[17] and the swift development in nanofabrication techniques such as focused ion beam (FIB) milling [18–20] and electron beam lithography (EBL)[21–23] have catalyzed the exploration of the man-made structural coloration.[24,25]

In this review, we will provide a synopsis of the recent research progress and achievements in nanostructure-based color filters. We will begin by defining several qualities that can be used as parameters to compare and analyze various nanostructure filters before moving on to different

*Address all correspondence to Yaping Dan, Email: Yaping.Dan@sjtu.edu.cn

sections of filters. The first type of structure we will discuss is plasmonic color filters as it is the recent trending topic among the scientists, followed by nanowire resonator filters and metamaterial filters. In the last section, we will include a brief study about QDs filters before we summarize this review and make a final comparison along with conclusion.

2 Figures of Merits

In order to make a fair comparison between different nanostructure color filters with different working principles, shapes, and form factors, it is useful to first define several figures of merits. We have summarized several qualities that hold the most importance in determining the performance of a filter. This in turn will give some insights on what kind of application is suitable for each type of nanostructure.

2.1 *Color Clarity*

An ideal color filter should have high color repetition, saturation, and purity as well as high contrast. These characteristics are usually related with the peak intensity, spectral bandwidth, and full-width half-maximum (FWHM). Higher transmission or reflection intensity will result in brighter color. Spectral bandwidth and FWHM are usually used to characterize linewidth, where thinner line, to some extent, is desirable as it will translate to lower crosstalk. Crosstalk is an unwanted phenomenon that suppresses the spectral responses of the affected color and enlarges the overlap in the signal of the other colors. Thus it is evident that the rise in crosstalk will attribute to the noise augmentation of the color correction mechanism, which results in worse signal-to-noise-ratio, degrading the color appearance. International Commission on Illumination (CIE) color diagrams govern the quantitative standard for this color clarity. On the other hand, smaller spectral bandwidth will enable not just the standard three-color imaging but also multispectral or hyperspectral imaging.[26]

2.2 *Spatial Resolution*

Spatial resolution is crucial as it affects how clearly we see objects and consequently is an important entity for every filtering and printing technologies. This figure signifies the pixel count available in a given dimension of an imaging part. Smaller pixel size leads to a higher spatial resolution. For color filters, the trend of maximizing the number of pixels and at the same time minimizing its size has resulted in smaller pixel pitch down to $<1\ \mu$m with pixel count inflated to above 40 million pixels. By expanding the spatial resolution to the submicrometer scale, we can incorporate ultrasmall product-identification and security methods that cannot be seen by naked eyes within the color decoration.

2.3 *Polarization Independence*

Generally, nanostructure color filters are expected to produce vivid colors, regardless of the angle, and illumination conditions in order to replace the current traditional filters. The intrinsic angular independence characteristic of pigments and dyes is appealing for devices that are required to display consistent "static" colors. Polarization sensitive structures may have their filtering performance degraded, e.g., lower color clarity at certain polarization. But polarization is like a coin with two faces. For some applications, it might be a big issue, whereas for some others it is highly desired if controllable since it might open doors for new additional features. Polarization itself can also be utilized as a basis for a tunable filter.

2.4 *Dynamic Tuning*

In recent years, there is surge of interest in developing actively tunable filters. As opposed to passive filters, in which the filtering capability was designed in prefabrication, actively tunable filters allow functional modifications in postfabrication via reversible processes. The color

tuning across the visible spectrum can be realized by applying external stimuli such as changing voltage bias, temperature variation, electrodeposition, or other electro-optic mechanisms. Dynamically tuning plasmon resonances while keeping the device composition and structure is sometimes desirable for achieving some interesting applications such as camouflage and cryptography. Dynamic tuning might be very useful for several applications requiring multifunctional and flexible device. This will also eliminate the need of refabricating a new filter since the change made to the device is completely reversible.

2.5 *Manufacturability*

Complexity of a structure will have a huge impact on the manufacturability. The higher its degree the more fabrication steps needed. Consequently, this quality is usually related to production cost. In general, complex structures will have higher associated fabrication costs. By minimizing the amount of composing materials, the manufacturability and recyclability of the filter can be improved. Designing a high-performance structure without creating a highly sophisticated structure is sometimes a big challenge. But it is in everyone's interests to keep the cost low and the throughput high to enable the widespread adoption in industry.

3 Plasmonic Color Filters

The whole idea of plasmonics is centered on a phenomenon known as surface plasmon resonance (SPR) that is excited often on metal surfaces by light illumination.[27–29] In fact, we can come across SPR in any material that has a negative real or small positive imaginary dielectric constant.[30] Under light illumination, the plasmon will oscillate locally on the surfaces of nanostructures, resulting in the electrons in conduction band moving in phase. The movement of electrons will electrically polarize the nanostructure surfaces,[31] creating a highly intensified local electric field that greatly increases the absorption and scattering cross section of the nanostructure. In recent years, numerous plasmon-assisted optical devices, such as waveguides,[32,33] photon sorters,[34,35] absorbers,[36,37] optical sensors,[38,39] and switches,[40] have been proposed and demonstrated experimentally. This technology has also been applied to other fields including material sciences, biochemistry, and information sciences and technologies.[41–43]

SPR-based color filter is one of the major applications of plasmonics. In comparison with organic color filters, this type of filter leads the race by far in terms of integration simplicity, tunability, color stability, and high resolution beyond the diffraction limit. In this section, we will briefly describe several examples of plasmonic color filters: nanohole arrays (NHA), nanowires, and other types of plasmonic color filters.

3.1 *Color Filters Based on Nanohole Arrays*

NHA are the most widely used nanostructure in plasmonic color filters. They are formed by patterning a metallic thin film using advanced lithography techniques such as EBL or FIB. Upon the illumination of light, the metallic subwavelength holes generate optical resonances in transmission, reflection, and absorption spectra, creating some interesting phenomena such as extraordinary transmission (EOT).[44] The EOT is a phenomenon where the optical transmittance is larger than the areal portion of the holes that allows the light to pass through. The characteristics of EOT are tunable by the physical geometry of the NHAs, including the period, diameter, and shape. For normal light incidence, the resonant wavelength of NHAs can be predicted by the following equation:

$$\lambda_{\text{peak}} = \frac{P}{\sqrt{L}} \sqrt{\frac{\varepsilon_m \varepsilon_d}{\varepsilon_m + \varepsilon_d}}.$$

For square lattice:

$$L = (i^2 + j^2)$$

For hexagonal lattice:

$$L = \frac{4}{3}(i^2 + ij + j^2),$$

where P denotes the periodicity, i and j are the array scattering order, ε_m is the metal dielectric constant, and ε_d is the dielectric constant of the material connected with the metal. It was studied that as the hole period and diameter increase, the transmission peak redshifts, and the transmittance strengthens, as shown in Fig. 1. This finding was further investigated by Si et al.,[45] where they fabricated annular aperture arrays in a gold film and successfully tuned its transmission resonance across visible range. Wavelength selectivity through these coaxial rings was achieved and precisely controlled to produce certain colors.

Studies about the hole geometry were also carried out by several research groups. Tang et al.[46] discovered that when the hole shape is designed to be an asymmetric C-shape aperture, the transmission spectrum is strongly dependent on the polarization of the incident light. What is more interesting is that the transmittance through the C-shape apertures is higher than the circular holes, although the open area for light transmission is the same for both geometries. When an array of such C-shape apertures is integrated on top of CMOS image sensors, the resultant photocurrent density is three times higher. In another investigation, Balaur et al.[47] examined the feasibility of cross-shaped NHA design for continuous color modulation by polarization. Cross-shaped apertures are deemed as the preferable structure for polarization responsive plasmonics due to their distinctive ability to facilitate different polarization states with tantamount efficiency.

Color filters based on NHAs are readily applicable in commercial products since the nanostructure is simple and easy to fabricate. Traditionally color filters based on organic dyes have size constraint where the filtering performance degrades as the filter size diminishes. Fortunately, this problem was solved by developing NHA-based filters where the filter size can be made as small as subwavelength while their filtering capability is maintained, as shown in Fig. 2.[48] Chen et al.[49] were the first to integrate the NHA-based plasmonic color filters on top of CMOS image sensors. EBL was applied to pattern NHAs in an aluminum film deposited on top of the CMOS photodiodes and the resultant clear-cut colorful logo is shown in Fig. 3. To illustrate that the NHA color filters will work properly when the array size scales down, a Bayer's RGB color pixel <1 μm is also shown in Fig. 4(a) and we can see that the filters still retain their colors despite of the pixel size shrinkage. For each color, the geometry of the NHAs will be different, as shown in the scanning electron microscopic images in Fig. 4(b). Apart from image sensors, Hu et al.[50] and Liu et al.[51] also integrated NHA filters onto OLED. They managed to accomplish a display with narrow bandwidth and high-purity RGB colors. Qiu et al.[52] demonstrated the practicability of

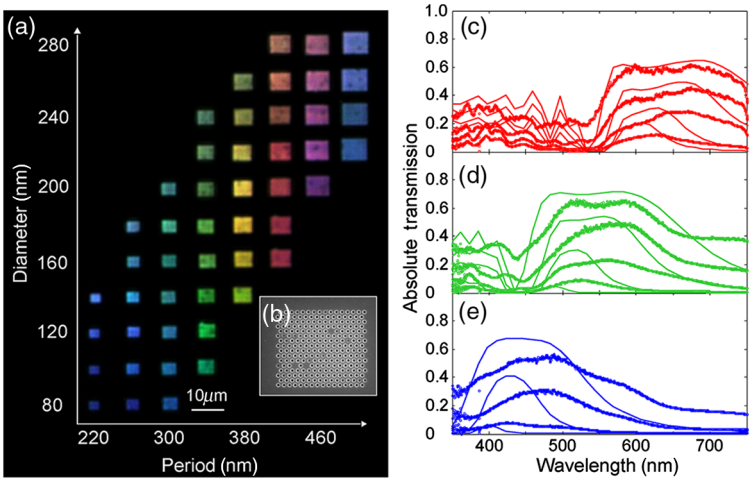

Fig. 1 (a) Relationship between periodicity and diameter of the holes with the color palette produced, (b) scanning electron microscopic image of a NHA, and (c)–(e) RGB filters dependence to resonance wavelength. Colors are produced in different wavelength regions. Both images were taken from Ref. 45.

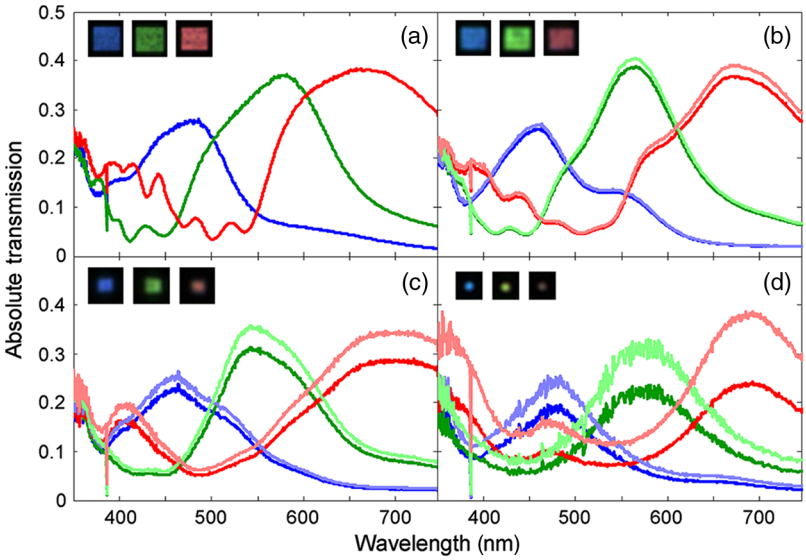

Fig. 2 RGB transmission spectra of hole array filters of different filter sizes of (a) 10 μm, (b) 5 μm, (c) 2.4 μm, and (d) 1.2 μm squared size filters. Insets: image of the filters under back illuminated microscope. The graphs are taken from Ref. 45.

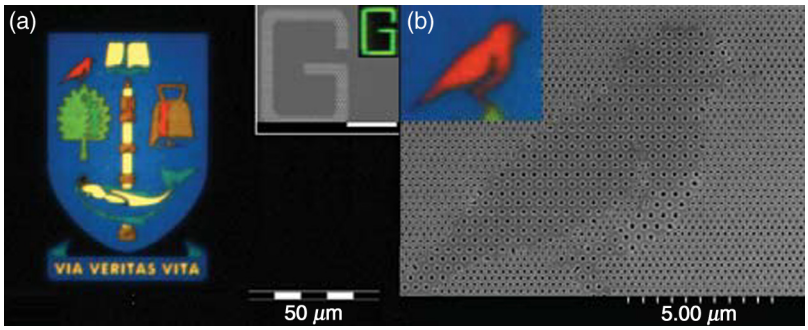

Fig. 3 (a) A well-defined colorful logo produced by NHAs and (b) partial detailed structure. The graphs are taken from Ref. 49.

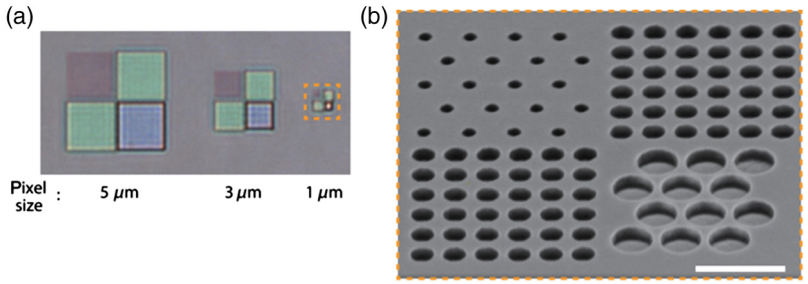

Fig. 4 (a) Progress in filter miniaturization down to 1 μm and (b) NHAs with various diameters and periodicities. Both images are from Ref. 49.

NHA filters for OLED application by further verification in structure's angle invariance, oblique incidence transmission efficiency, and polarized incidence independence.

Finally, the biggest disadvantage of metal-based NHA is their considerably low transmittance (<60%). In order to alleviate this problem, Horie et al.[53] proposed a polysilicon film-based NHA. In their design, the NHA filters are fabricated in an 80-nm-thick polysilicon film on top of 115-nm-thick SiO_2 substrate. This device achieved a transmittance of 60% to 80% and

virtually unaffected by polarization up to 20-deg angular range of incident lights. Another downside of NHAs is that the transmission characteristics are dependent, to some extends, on the angle and polarization of the incident light. In order to mitigate this setback, Labeke et al. schemed an angle and polarization independent filter.[54] Fouladi et al.[55] had also devised a dual mode operation filter, which is polarization insensitive. A complete study of the angle sensitivity, size effect, and spatial optical crosstalk of NHA filter was also carried out by Yu et al.[56]

3.2 *Color Filters Based on Nanogratings*

The anomaly of optical diffraction gratings was first revealed by Wood.[57] Decades later, Knop[58,59] investigated the diffraction grating effect of 1-D metal structures for color filtering application, opening the field of subwavelength grating (SWG) filters. SWG outperforms traditional grating because it does not generate higher diffraction orders due to the fact that the period is smaller than the wavelength of an incident light.[60] In this case, the grating behaves as a homogeneous layer with the effective refractive index valued between the material and the surrounding index. A selective spectral response can be achieved by means of the guided mode resonance (GMR) effect attributed to the coupling between incident light and the periodic structure.[61] The coupling between the periodic elements will diminish the radiative loss and creates localized electric field orders of magnitude stronger than that of an individual structure. When the period of an SWG on a planar waveguide satisfies the GMR condition, the grating works as a high-efficiency band-stop filter at the resonant wavelength. Band-stop filters that satisfy the GMR condition can achieve narrow and broad bandwidths using aluminum as the SWG material owing to its cost effectiveness, easy integration with other devices, and CMOS compatibility.[62] It is also possible to realize bandpass color filters by covering metal SWG with an appropriate dielectric.[63] This phenomenon has been observed by several research groups.[64–70]

Wang et al.[71] developed subwavelength metal grating-based plasmonic color filter incorporating a free-standing membrane waveguide that is capable to achieve 70% transmission efficiency in the visible spectrum. Because of the transparent substrate omission, the thickness can be reduced to <200 nm. Arbitrary micron-scale multicolor patterns were achieved by designing the plasmonic filters with various grating periods as illustrated in Fig. 5(a). Transmission spectra and mapping transformation to CIE1931 color space of this filter are shown in Figs. 5(b) and 5(c). Additionally, the FWHM of the transmission spectra can be tuned by controlling the MgF_2 cladding layer thickness. The science behind it lies within the metallic resonant waveguide grating theory.[72]

In recent development, Shrestha et al.[73] demonstrated highly efficient dynamic subtractive color filters made of a dielectric-loaded aluminum nanowire array. Figure 6(a) illustrates the designed dynamic color filters and Fig. 6(b) shows the SEM images of the fabricated filters with various periodicities. Dynamic color filtering was accomplished by a combination of plasmonic resonance and GMR. This combination results in a continuum of customized color that is dependent on the incident light polarization as shown in Fig. 6(b). The transmissions were

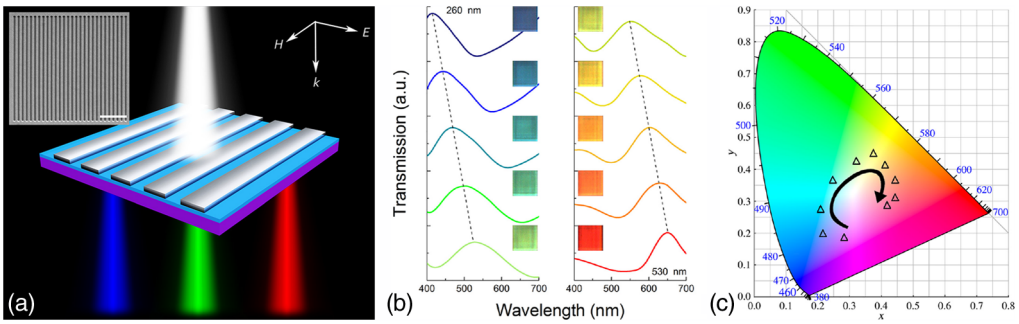

Fig. 5 (a) Schematic diagram of a nanograting filter structure. Inset presents SEM image of the fabricated structure (scale bar = 2 μm). (b) Relationship between spectra of colors and the grating period of filter. Periodicity was set 260 to 530 nm, with 30 nm increase. (c) Mapping transformation of the measured spectra in the CIE1931 color space. Images are from Ref. 71.

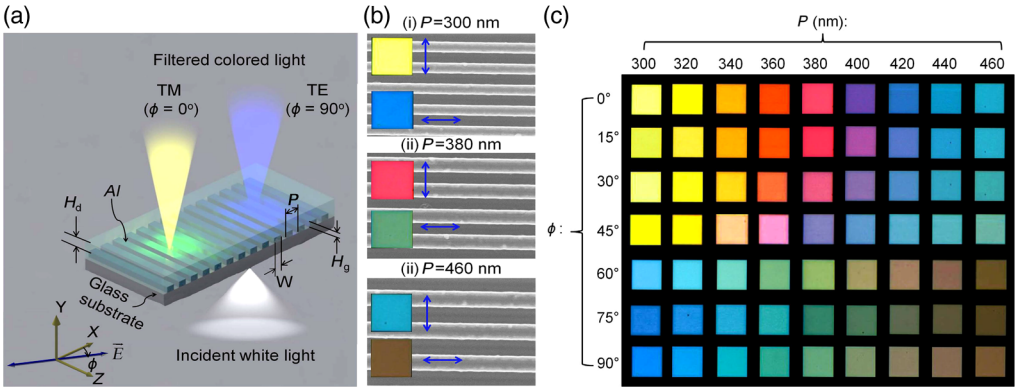

Fig. 6 (a) Schematic view of the structure proposed by Shretsa et al., (b) SEM images of the fabricated filters, and (c) color palettes produced by nanograting filters are shown to be dependent on both periodicity and polarization degrees. Images are from Ref. 73.

observed to be above 80% for both transverse magnetic (TM) and transverse electric (TE) polarization. Most importantly, this device accommodates two degrees of freedom to adjust the transmitted colors in transmission mode. One is periodicity, which is fixed before fabrication, and the other one is incident light polarization, which enables color-tuning possible even after fabrication.

An interesting new structure based on out-of-plane lattice plasmons was also reported by Taghinejad et al.[74] shown in Fig. 7. In fact, the terms "in-plane" and "out-of-plane" resonances were first proposed by Odom et al.[75] for characterizing plasmon excitations in and perpendicular to the array plane, respectively. This 2-D plasmonic grating structure made of nanopatches (NP) shows sharp plasmonic crystal (PC) resonances through a broad wavelength range of 230 nm, with a small FWHM of about 6 nm. The PC resonance was formed by the coupling of the neighboring out-of-plane NP dipoles within the lattice plane under angled exposure. The incidence angle can be used to systematically tune the peak of resonance. By exploiting the strong interaction between the excited out-of-plane dipoles within the NP and the induced image dipoles of

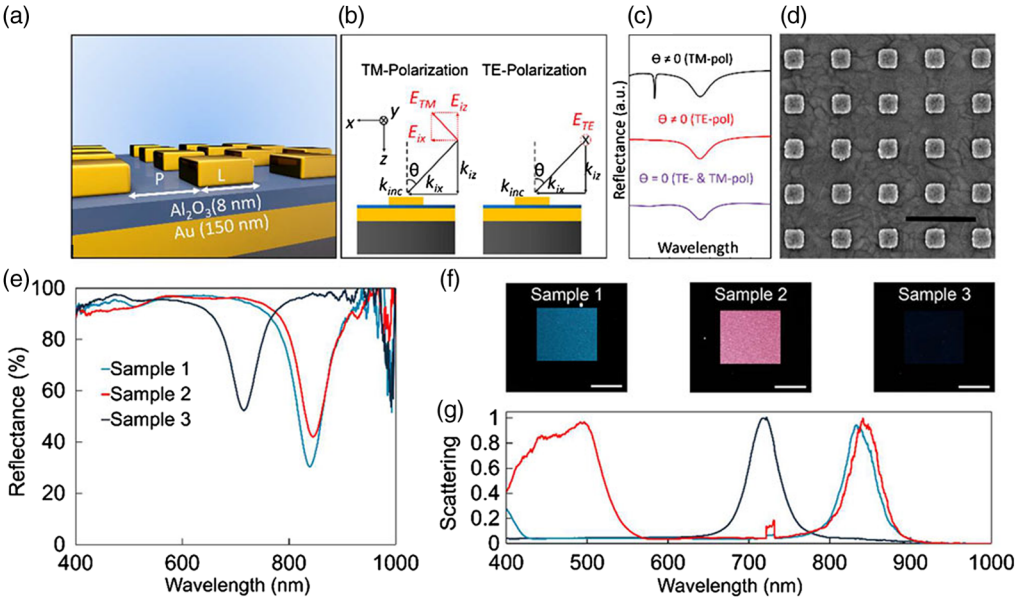

Fig. 7 (a) Illustration of the 2-D array structure, (b) electric field components and polarization states, (c) optical responses from different angles and polarization, (d) SEM image of the fabricated samples (bar = 500 nm), (e) reflection spectra of three fabricated samples, (f) dark-field images of the three samples (bar = 100 μm), and (g) normalized dark-field scattering spectra. Images are from Ref. 74.

the Au film underneath, it was possible to obtain remarkably thin PC resonances with just 30-nm-thick NP. Additionally, the PC exhibited by this NP allows for a plasmonic Fabry–Perot-like resonance, which may be utilized to produce complex Fano-type lineshapes.

Using the same out-of-plane principle, Zhou and Odom[76] fabricated a filter based on subradiant plasmon with a narrow resonant linewidth of 5 nm that is tunable by altering the thickness (>100 nm) of 2-D gold nanoparticles array. The out-of-plane structure was employed to create dark and subradiant lattice plasmon modes. These modes can be either passively controlled by tuning the structure thickness or actively adjusted by varying the angle of incidence. A Fano-type spectral shape characterized with asymmetric peak-and-dip feature was the evidence of the interference among the subradiant (narrow) out-of-plane and superradiant (broad) in-plane resonance of the lattice plasmon. Since thickness-controlled arrays of nanoparticle can be easily fabricated on different substrates at wafer-scale, this method opens a door for applications in subradiant plasmons localized surface plasmon sensors, surface enhanced Raman spectroscopy, and plasmon-enhanced nonlinear nano-optics. The 1-D version of the nanogratings was also investigated and it was found tunable over 400-nm range in the visible wavelength, much better in performance than the previously proposed 2-D structure.[77] The improvement is attributed to the lower structure symmetry in respect to the higher dimension one. Huttenen et al.[78] further explored the optical properties of in-plane and out-of-plane structures, in which they found the later have stronger polarization dependence than the former due to its omnidirectional coupling capability inside the array plane. The necessary conditions to achieve out-of-plane resonance were also analyzed and formulated by Li.[79] The essential factors for optimization include the structure thickness and the incidence angle, homogeneous dielectric environment, and specific array period.

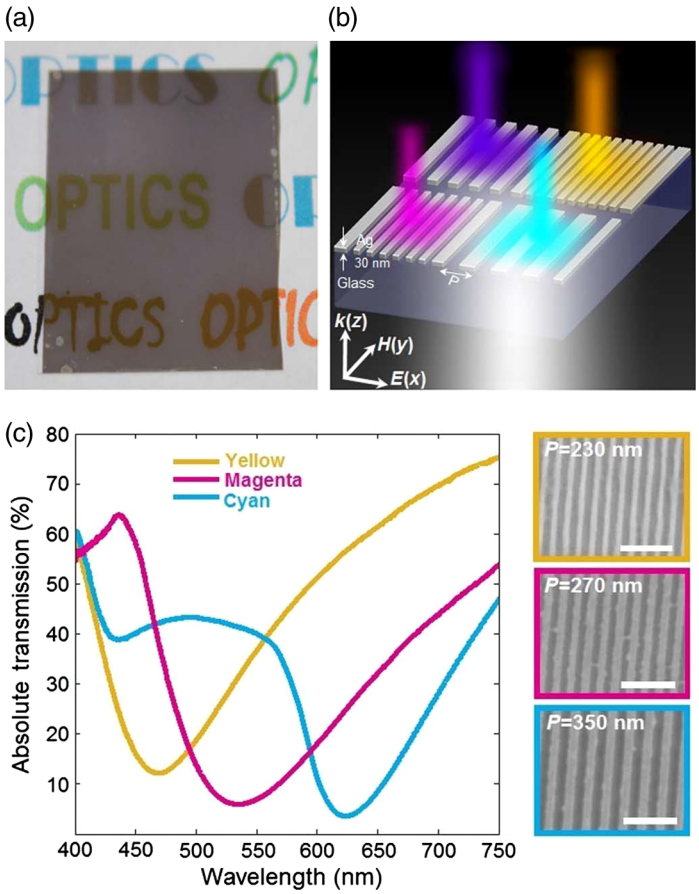

Fig. 8 (a) A photograph of a 30-nm-thick semitransparent Ag film deposited on a microscope glass slide, (b) illustration of plasmonic subtractive color filters made of ultrathin Ag nanogratings, and (c) measured TM transmission of YMC spectra. Images are from Ref. 80.

On the other hand, Zeng et al.[80] revealed a plasmonic subtractive color filtering (SCF) scheme that makes use of the peculiar phenomenon of extraordinary low transmission (ELT) through an ultrathin patterned metal film. As opposed to the EOT phenomenon, which can be seen through a thick metal film (with respect to its skin depth), ELT can be observed in an ultrathin metal film whose thickness is less than or equal to its skin depth. The color filtering mechanism of SCF is totally contradistinctive from those of contemporary plasmonic additive color filters. In SCF, the reflection and absorption are increased at the resonance wavelength for normally incident light polarized along the x direction (TM polarization). This results in a transmission minimum, which is contrary to the renowned EOT phenomenon that shows enhanced transmission maximum at the resonance wavelength in optically thick patterned metal films. The dependence of the transmission minimum wavelength on film thickness and nanograting period was derived by Hu et al.[81] Figure 8 exhibits the image of a semitransparent Ag film placed on a microscope glass slide, design of the plasmonic subtractive color filters made of ultrathin Ag nanogratings and its transmission spectra.

Plasmonic SCFs can adequately achieve filtering function with as few as two nanoslits, by virtue of short-range interactions of SPRs among nearest-neighbor nanostructures at the ELT resonances. This allows extremely compact pixel sizes roughly equal to the optical diffraction limit ($\lambda/2$, ~200 to 350 nm), a standard that defines the maximum attainable optical resolution.[82,83] Additionally, their unusual polarization-dependent characteristics made it possible for this structure to switch functions between color filters and all-wavelength-transparent windows depending on particular polarizations, unlocking possibilities for high-definition translucent displays.

3.3 *Other Type of Plasmonic Color Filters*

Apart from the two most popular plasmonic structures presented in Secs. 3.1 and 3.2, there are also other interesting architectures used for color filtering. Xu et al.[84] proposed very compact plasmonic nanoresonators made of subwavelength metal–insulator–metal stack arrays. This filter utilizes selective conversion between free space waves and spatially confined modes in the nanoresonators to spectrally disperse light. Figure 9(a) shows the schematic diagram of the nanoresonator filter. Figure 9(b) illustrates the time-average magnetic field intensity and electric displacement distribution. Analogous to wire-grid polarizers demonstrated by Wang et al.,[85] this filter also strongly reflects TE-polarized light. It implies that this device can act as a color filter and a polarizer at the same time, serving as an ideal structure for LCD, which normally requires a separate polarizer layer. Moreover, a separate transparent conductive oxide layer employed in LCD module might also be omitted since the functionality can be substituted by the Al grating conductive attributes.

Coaxial-aperture-based plasmonic nanostructures that operates in both reflection and transmission mode [Fig. 10(a)] was also proposed by Jiang et al.[86] An accurate control of plasmonic resonances in the visible regime can be achieved by precisely controlling the etching depth of the coaxial apertures. In Fig. 10(a), the film was milled by FIB system. As seen in Fig. 10(b), shallow etch will produce brighter colors in the reflection mode. These colors turn darker and

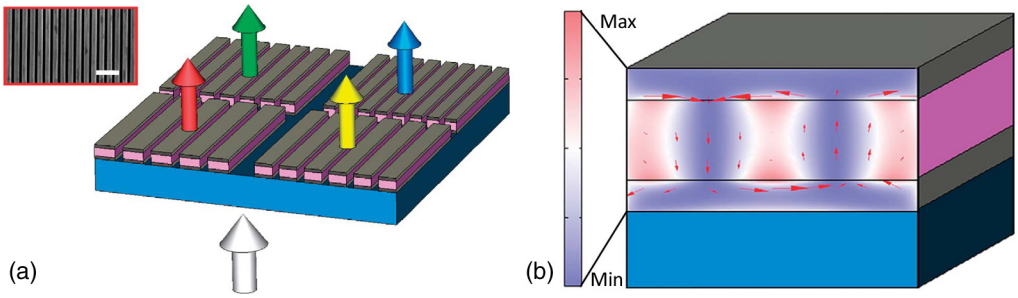

Fig. 9 (a) Schematic diagram of plasmonic nanoresonators and (b) cross section of the time-average magnetic-field intensity and electric displacement distribution (red arrow) inside the MIM stack. Images are from Ref. 84.

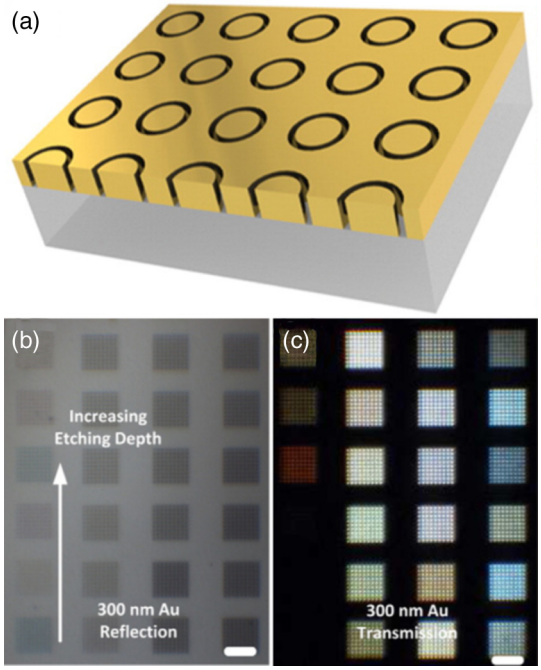

Fig. 10 (a) Illustration of the coaxial aperture structure proposed by Jiang et al. and (b) and (c) colors produced by the reflection and transmission mode of the filter shown in (a), respectively. Images are from Ref. 86.

eventually black as the etching depth increases. Conversely, in transmission mode, the colors get brighter with deeper etch [Fig. 10(c)]. For shallow etches, the colors appear to be black because the film is opaque for low-depth coaxial apertures.

There are also some other interesting structures such as nanopatch,[87] nanorod,[88] and nanovolcano.[23] However, we cannot go through each of them due to space limitation. Current dynamic plasmonic displays cover the entire visible spectral range by varying the plasmonic structure parameters or by switching the surrounding medium properties and filtering the colors of different polarizations. The full color display capability can be reached but the color vibrancy needs improvement. Such improvement requires the smart design of nanostructures and the exploration of novel materials that support optical resonances. The prospect for new types of plasmonic color filters is bright for applications in surface decoration, digital display, and even spectral analyzer. We may expect more efficient and streamlined structures to emerge in years to come.

4 Nanowire Color Filters

In general, refractive index is inversely proportional to the electrical conductivity of material. It means that metals and insulators have the highest and lowest refractive index, respectively. As a result, metallic nanowires have the strongest confinement of light and therefore can make very small but lossy color filters. Insulating nanowires have the weakest confinement of light, which makes them a good candidate for waveguides instead of color filters. Semiconducting nanowires have relatively high-refractive index. Light propagation in the nanowires depends on the photonic confinement, which is determined by the cross-sectional size[89,90] and refractive index of the nanowire cavity. Low-propagation losses combined with high confinement of light have made semiconducting nanowires as one of the best choices for nanoscale confinement waveguides[91–95] and color filters.[96] When the light is coupled into the nanowires, two optical modes will be created. One is leaky mode resonances (LMR), in which light is circularly resonating. The other mode is wave-guiding modes, in which light is propagating along the nanowire axis. Both of these modes will create color selectivity and can be used for color filtering.

4.1 *Horizontal Nanowires*

For horizontal nanowires, LMR will be created when the light is launched perpendicularly from the top.[97] In this case, nanowires can be treated just like a miniaturized form of microcylinder resonators that utilize multiple total internal reflections within the cylinder boundary to trap light in circulating orbits, creating some spectral selectivity effect. The classical waveguide theory is the basis for the mechanism of highly confined modes in microscale dielectric resonators and optical fibres. LMR that arises in an infinitely long dielectric cylinder with radius "r" can be predicted by solving Maxwell's equations using the suitable boundary condition, shown as the following:[98]

$$\left(\frac{1}{\kappa^2}-\frac{1}{\gamma^2}\right)^2\left(\frac{\beta m}{r}\right)^2=k_0^2\left[n^2\frac{J'_m(\kappa r)}{kJ_m(\kappa r)}-n_0^2\frac{H'_m(\gamma r)}{\gamma H_m(\gamma r)}\right]\times\left[\frac{J'_m(\kappa r)}{kJ_m(\kappa r)}-\frac{H'_m(\gamma r)}{\gamma H_m(\gamma r)}\right],$$

where n, κ and n_0, γ are the refractive index and transverse wave vector inside and outside of the cylinder, respectively, β is the wave vector across the axis of the cylinder, and k_0 is the wave vector in free space. J_m and H_m are the m'th order Bessel and Hankel function of the first kind, whereas J'_m and H'_m signify the differentiation in respect to associated variables. Above formulation can be divided into two cases for normal incidence (where $\beta=0$) of a cylinder in vacuum (where $n_0=1$). The first one is purely transverse-magnetic modes and the second is transverse-electric modes, in which the magnetic fields are in the plane normal to the nanowire axis $[nJ'_m(nk_0r)/J_m(nk_0r)=H'_m(k_0r)/H_m(k_0r)]$ for the former and the electric fields is normal to the nanowire axis $[J'_m(nk_0r)/nJ_m(nk_0r)=H'_m(k_0r)/H_m(k_0r)]$ for the later. Thus we can see that nanowires incline to have a finite amount of TM and electric LMRs that scales up with the radius enlargement.

Cao et al.[99] showed that resonant field enhancements within horizontal semiconductor nanowires can be utilized to adjust and strengthen their absorption spectra. The analysis was carried out with a set of horizontal germanium nanowires with various diameters grown using

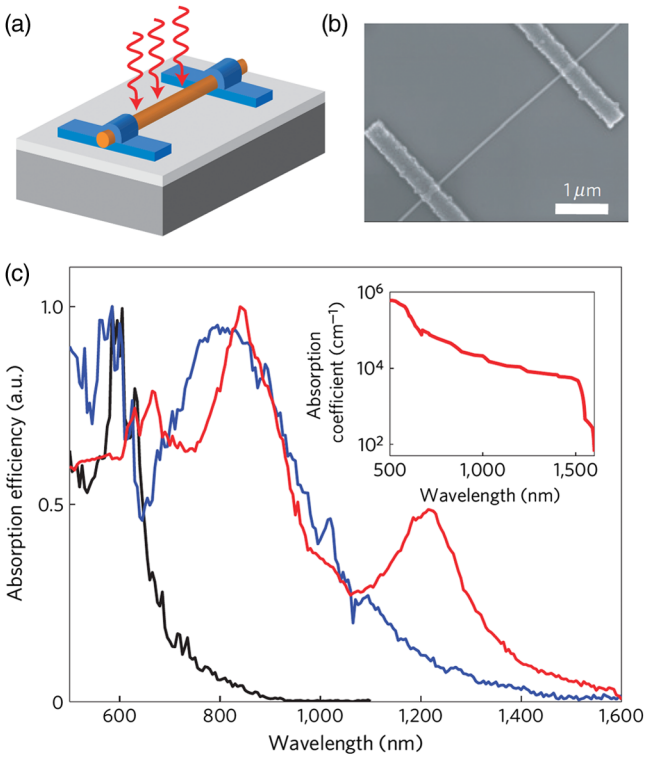

Fig. 11 (a) Illustration of a germanium nanowire device, (b) SEM image of a 25-nm-radius germanium nanowire device, and (c) measured spectra of absorption efficiency for radii of 10, 25, and 110 nm, denoted by black, blue, and red, respectively. Images are from Ref. 99.

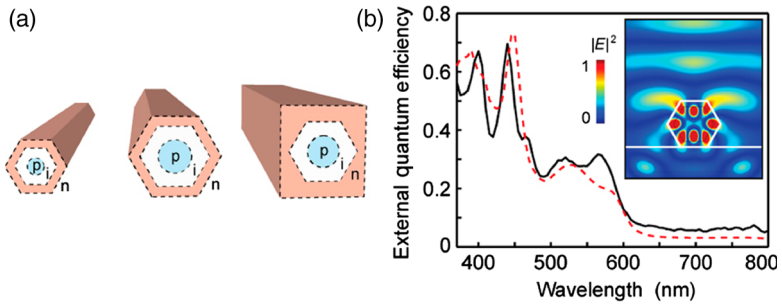

Fig. 12 (a) Schematic illustration of p/i/n Si nanowire structures and its variations in terms of size and shape. (b) EQE of coupling between a vertically incident plane wave and highly confined resonant modes within an Si nanowire. Inset: electric field intensity of the nanowire. Images are from Ref. 101.

an Au-catalyzed chemical vapor deposition process. Figure 11 exhibits the filter structural schematic along with the SEM image and light absorption spectra of a horizontal germanium nanowire. This idea of integrating LMR with semiconductor architecture can also be used to manipulate spectral absorption properties of other semiconductor materials and object geometries.[100]

The study of a synthesized core/shell Si nanowire devices with various dimensions and cross-sectional geometries was also carried out by Kim et al.[101] They demonstrated that differences in shape and size have considerable impact on the external quantum efficiency (EQE) spectra of single-nanowire photovoltaic devices as presented in Fig. 12. It can be inferred from the graph that the larger the size of the hexagonal nanowire, the greater the number and wavelength of resonances will be. Moreover, nanowire cross-sectional geometry can be transformed from hexagonal to foursquare by taking advantage of the enhanced facet shell growth. An improved EQE characteristic at long wavelengths was observed in the square-shaped nanowire because of resonant modes excitation inside this highly symmetrical geometry. Due to the universality of this concept, analogous size and geometry controlled optical resonances can also be found in other nanowires materials with high refractive index like Ge, GaAs, and PbS. Further research in this topic might open doors for cutting edge approach in the manipulation of absorption properties, which play important roles in regulating color filtering capability in nanowire materials.

4.2 *Vertical Nanowires*

Vertical nanowires rely on wave-guiding modes, in which light is propagating along the nanowire axis.[102,103] In comparison with bulk materials and thin films, vertical nanowire arrays have exhibited better optical absorption, thanks to the near-field coupling and the resonant excitation of the transverse optical modes inside the cylindrical structure of the nanowires. Additionally, the exceptional reflection and absorption properties are attributed to the longitudinal mode excitations through the Fabry–Perot cavities built by the top and bottom interfaces of the nanowires. An in-depth explanation of the physical mechanism for this filtering method has been elaborated by Crozier et al.[104]

Ye et al.[105] have shown that a signal at a given wavelength can be filtered by adjusting the width of an individual nanowire waveguide to the critical point through the propagation orientation. Seo et al.[106] validated the feasibility of using vertical silicon nanowires to produce a range of bright colors spread across the entire visible regime, despite the gray color observed from a bulk silicon. The SEM image of the nanowire array is shown in Fig. 13(a). The resonant wavelength of this filter is determined by the nanowire radii, in which a bigger radius will redshift the graph as shown in Fig. 13(b). Although the nanowires were constructed as arrays, the dynamic colors seen are actually produced by the guided mode features of every single nanowires instead of diffractive or scattering response of the array. Therefore, colorful spatial patterning is possible because of the nanowire ability to independently determine its own color and stay unaffected by its adjacent structures.

In particular, semiconducting nanowires are capable to produce electron–hole pairs upon illumination of the coupled light. If the nanowires are devised into active devices such as pn

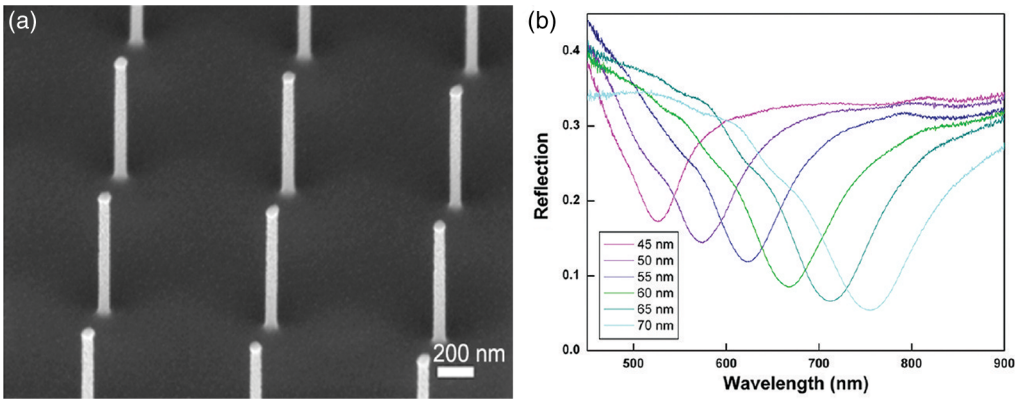

Fig. 13 (a) Nanowire array fabricated by Seo et al. and (b) measured reflection spectra of nanowire arrays that show relationships between spectral dip and nanowire radii. Images are from Ref. 106.

junction diodes, filter-less color pixels can be created.[106] Park et al. proposed an all-silicon vertical nanowire color filter with integrated photodetectors whose spectral responses are regulated by nanowire radius that were fabricated as shown in Fig. 14(a). Attributed to the extraordinary optical properties of semiconductor nanowires, spectral absorption of this device can be devised to create a filter-less color imaging. Unlike filter-based methods, the absorbed light is transformed into photocurrent and consequently facilitates immense photon efficiency. A full color image produced by this device is shown in Fig. 14(b).

Yoon et al.[108] further probed the optical characteristics of vertical nanowire filters by exploring asymmetric nanowire structures. It was found that compared to symmetric and top-wide asymmetric nanowire, bottom-wide asymmetric nanowire transmits and reflects less undeviating incident light because of its wide bottom and narrow top cross sections. As a result, higher EQE peaks can be achieved while at the same time still maintaining the waveguide properties. Additionally, a polarization resolved imaging without the need of a polarizer is also possible by employing vertical nanowire with elliptical cross section.[109] Unlike the conventional approaches in which the absorbed light by polarizer is discarded, elliptical nanowire turns the light absorbed into photocurrent, which paves the way for a highly efficient polarization-resolving pixels.

5 Metamaterial Color Filters

Metamaterials are artificial micro- or nanostructures consisting of metallodielectric subwavelength elementary units that are periodically or haphazardly arranged.[110] The precise shape, size, orientation, and arrangement of the composing elements create bizarre properties that are nonexistent in natural materials by manipulating electromagnetic waves. We may consider the whole set of these tiny elements as one entity with effective material properties at the macroscopic level.[111] For example, appropriately designed metamaterials can influence the phase of electromagnetic waves to produce some extraordinary behavior never seen in bulk materials such as

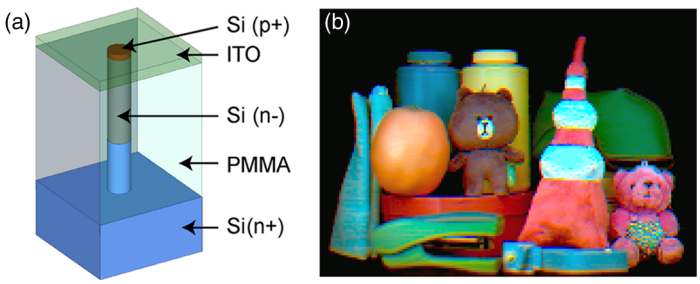

Fig. 14 (a) Schematic structure of vertical silicon nanowires-based p–i–n photodetectors and (b) resulting color image produced. Images are from Ref. 107.

negative refractive index.[112] This seemingly facile but mighty notion also unlocks the possibility of numerous other innovative and extraordinary optical such as extremely large refractive index, zero reflection through impedance matching, and perfect absorption. A thorough explanation about this particular field has been covered in other reviews.[113–115] This segment will be dedicated for a brief introduction of recent advances in metasurfaces for color filters.

Metasurfaces can be regarded as an artificial layer metamaterial with a two-dimensional array of nanoscale scatterers on its surfaces. When light impinges on the surfaces, the wave front will be manipulated by the nanoscatterers, creating similar negative refraction, and reflection as in metamaterials. Compared to metamaterials, metasurfaces have unique advantages. First, a lower dimension may translate to reduced fabrication complexity and lower Ohmic loss of metals, which eventually mean cheaper manufacturing and better performance, respectively. Second, the 2-D structures are more versatile, flexible, and much easier to fabricate. Depending on the wavelength, polarization, or efficiency requirements, we can adopt a specific structure for a particular application. Finally, metasurfaces are easier to integrate on-chip with quasiplanar optical devices. For miniaturized photonic systems, in particular color filters, this quality is highly advantageous. As a result, many research groups have shifted their attention to metasurface filters especially those employing aluminum and silicon due to their maturity in the industry.

Yue et al. first manifested highly efficient cyan, magenta, and yellow (CMY) subtractive filters by integrating silicon–aluminum (Si–Al) hybrid nanodisk (ND) metasurfaces onto an Si substrate[116] as shown in Fig. 15(a). The Si–Al hybrid ND color filters outperform conventional Si nanowire filters in terms of color purity due to their narrow bandwidth and close-to-zero reflectivity at resonance wavelength [Fig. 15(b)]. Upon light illumination, each of the hybrid-NDs contributes to the excitation of magnetic dipole (MD) resonance by the means of Mie-scattering. The light enhanced by the resonance is efficiently coupled to the substrate, as a result of which the reflectivity is suppressed. In addition, the resonance can be tuned across the visible spectrum by changing the hybrid-ND diameter. Because of this tunability, it is possible to realize a complete color palette having a high color purity and a wide range of color gamut. The prospective applications for this device might include but are not limited to photorealistic high-resolution color printing and holographic displays.

Another interesting structure based on plasmonic V groove metasurfaces out of an aluminum film was also proposed by Wang et al.[117] This structure was fabricated by a one-step FIB milling process. An extensive color palette was successfully attained by tuning the depth of the groove while preserving groove period constant.

One of the most fascinating capabilities of the metasurface-based color filters is the prospect for real-time color tuning. Wang et al.[118] suggested an approach to enable light manipulation in real time to promptly blend with background color in the surroundings. This was realized by utilizing both of bimetallic Au/Ag core–shell nanodome array metasurfaces and electrochemical bias shown in Fig. 16(a). The colors produced by the filter are mainly emerged from the plasmonic absorption and reflection bands of the Au core. Electrodeposition is utilized to control the Ag shell thickness on the Au core by employing gel electrolyte containing Ag^{+} ions. This

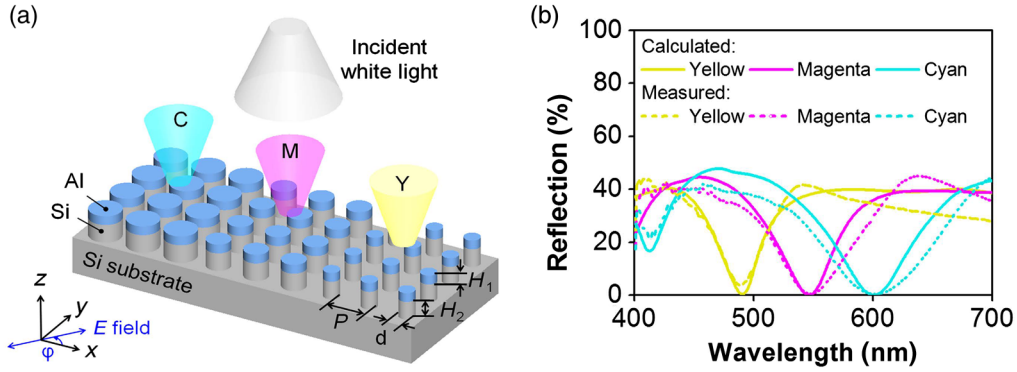

Fig. 15 (a) CMY color filters incorporating an Si–Al hybrid-ND metasurface structured on an Si substrate and (b) reflection spectral responses of the CMY devices in case of normal incidence. Images are from Ref. 116.

method of electrodepositing and removing Ag shells on plasmonic Au nanodomes creates a reversible plasmonic cell that enables a continuous color tuning across the visible wavelength. Figure 16(b) exhibits the dependence of the filter reflection spectra on the Ag deposition time. The resonant peak was observed to shift toward lower wavelength as the Ag deposition time increases. A biomimetic mechanical chameleon covered with the proposed metasurface color filters was devised and the camouflage effect was demonstrated in Fig. 16(c). Even though this chameleon was shown only to work against three primary colors (RGB) backgrounds, but in the future this technology can also engage with more sophisticated surroundings and pave a new way for man-made active camouflage. Other actively tunable structures were also proposed, such as one made of TiO_2 nanoblocks, which utilizes injection of solution with different refractive indices[119] and another structure utilizing liquid crystal as the tunable medium.[120]

On the other hand, the performance of metasurface color filters based on metal-dielectric plasmonic nanostructures is often deteriorated by the metal absorption loss.[121,122] To alleviate the metallic loss, high-index dielectric materials such as semiconductors that depend on electric and MDs were suggested as the main substitute to metallic metasurfaces.[123–128] Silicon is regarded as one of the top options to build dielectric metasurfaces because of its CMOS compatibility.[129]

Park et al.[130] manufactured and analyzed high-performance dielectric metasurface color filters made of hydrogenated amorphous silicon (a-Si:H). The metasurface consists of a-Si:H nanodisk arrays on top of a polymer film, shown in Fig. 17(a). The a-Si:H nanodisks are designed to independently sustain electric and MD resonances through Mie scattering, which gives rise to wavelength-dependent filtering features shown in Fig. 17(b). Various bright subtractive colors were realized by tuning the structural parameters such as diameter and periodicity of the a-Si:H nanodisk as can be seen in Fig. 17(c).

A polarization-dependent color filter was also developed by Vashistha et al.[131] The filter was made of all-dielectric metasurfaces based on asymmetric cross-shaped Si nanoantennas as shown in Fig. 18. An arbitrary color can be generated by properly sizing the rectangular segments of the asymmetric cross. The length ratio of the shorter (y axis) to the longer (x axis) section allows for a wide tuning range of resonance wavelength. Because of the asymmetric feature of the cross shape, the color tunability of the filter is highly dependent on the incident wave polarization. Additionally, the color filter is designed to operate in both transmission (for CMY) and reflection mode (for RGB), creating extra freedom for color tuning, resulting in a broader color palette. Another interesting polarization-dependent structure utilizing titanium oxide was also proposed

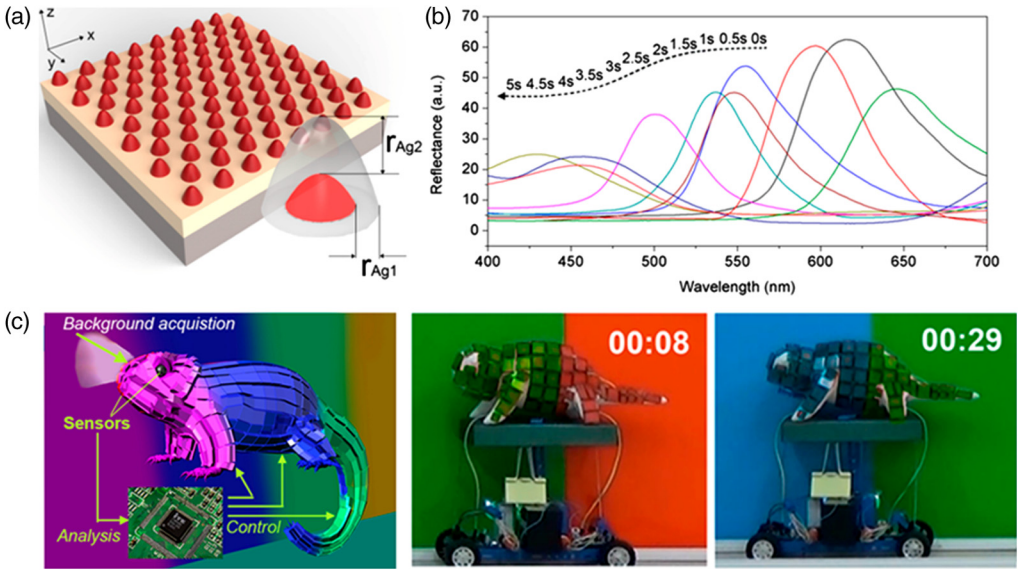

Fig. 16 (a) Schematic of the structure proposed by Wang et al., (b) experiment result showing the tunability of the structure, and (c) demonstration of the mechanical chameleon. Images are from Ref. 118.

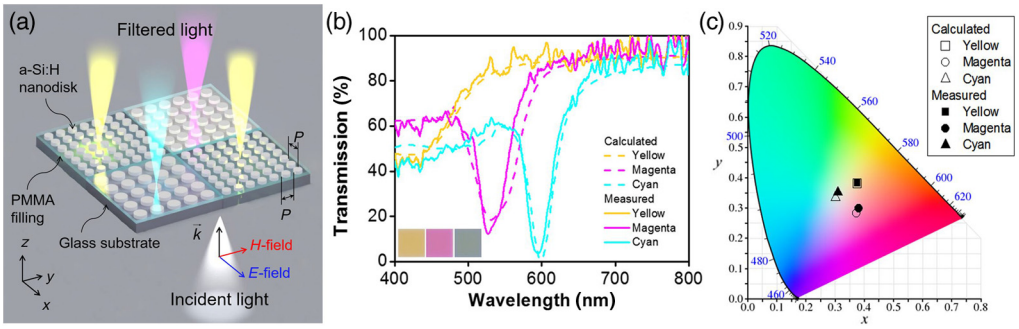

Fig. 17 (a) Schematic diagram of the proposed a-Si:H nanodisk and its experimental results (b) and (c). Images are from Ref. 130.

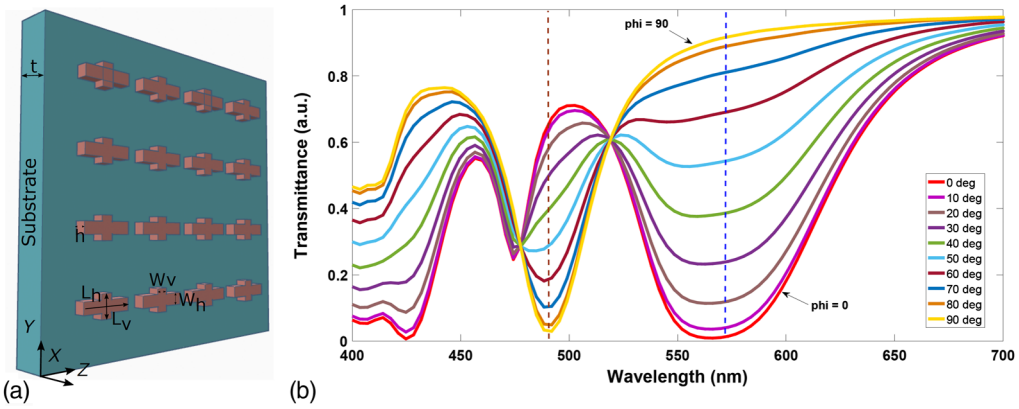

Fig. 18 (a) Metasurface composed of nonsymmetric Si nanoantennas grown on top of quartz substrate. Inset: schematically shows wave propagation in case of x polarized ($\Phi = 0$ deg) and y polarized ($\Phi = 90$ deg) normally incident wave. (b) Shift in transmittance spectra when Φ is varied from 0 deg to 90 deg). Images are from Ref. 131.

by Yang et al.[132] This device enables tuning of color hue and saturation at the same time under two orthogonally polarized incident lights.

6 Quantum Dots Color Filters

QDs are nanoparticles with radii ranging from 1 to 10 nm. These "dots" are smaller compared to the bulk exciton Bohr radius, resulting in quantum confinement of charge carriers that converts the continuous energy band structure into a discrete one. In general, a smaller size will induce a stronger quantum confinement and consequently a larger effective bandgap.[133] QDs can absorb and emit light upon illumination. A larger effective bandgap will blueshift both optical absorption and emission.[134] Additionally, QDs possess superior photostability compared with traditional dyes.[135,136] As a result, QDs have been developed for a wide range of applications from light emitting devices, solar cells to color filters.

In the conventional LCD, the liquid crystal color filters have a relatively narrow color gamut. QD color filters have a wider color gamut due to the tunable emission wavelength and purer color characterized by the narrow FWHM of about 20 to 30 nm. Zhang et al.[137] pioneered the use of QD color filters for a liquid crystal panel comprising a plurality of pixels as illustrated in Fig. 19. In this work, a blue LED was used to excite red and green QDs that will emit bright red and green colors. Part of the blue light that was not absorbed by the QDs will be filtered by the dye color filters. These hybrid color filters will create three highly saturated primary colors with high color purity. A complete basic working principle has also been reviewed previously.[138]

Liu et al. proposed a well-arranged QD array, in which RGB color separation was also realized through excitation by blue back light.[139] To suppress ambient excitation and color crosstalk,

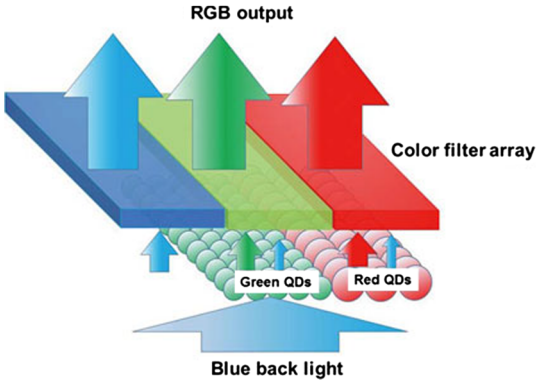

Fig. 19 Quantum dot filter illustration from Ref. 139.

QDs array was assembled on top of conventional color filters to realize 99.4% adobe RGB color gamut. As we can see from Fig. 20(a), blue light crosstalk is greatly reduced in QDs-enhanced color filter arrays. The color gamut achieved by the emission spectrum of the proposed filter can also be seen in Fig. 20(b). Unlike plasmonic color filters, the transmission efficiency of QD filters does not rely on the geometrical arrangement order of filtering elements. Instead, it is determined by the color conversion efficiency of QDs. The color conversion efficiency can be improved by enhancing the quantum yield and color separation efficiency. In addition, the conversion efficiency can be further increased by increasing the number of QDs layers[140] and recycling the blue light.[141]

Later that year, Kim et al. proposed an LCD structure employing a short-pass filter (SPF) and a patterned QD film capable of realizing a very wide color palette shown in Fig. 21.[142] The SPF is a kind of distributed Bragg reflector, which is composed of multiple pairs of two alternating layers with different refractive indices.[143] It has wavelength-dependent transmission characteristics that can be altered by changing the material and thickness of the dielectric layers. The patterned QD film contributes to the realization of 90% of the Rec. 2020 color gamut, equivalent to 127.5% of CIE 1931. Additionally, the optical intensities of the red, green, and blue spectra were enhanced to 1.63, 1.72, and 2.16 times compared to the conventional LCD values, respectively. This was a result of separated emission of the red and green patterned QD film and reflection of the red and green light to the forward direction by the SPF.

Polarization loss in QDs emission may undermine the QDs array functionality in LCD tricolor separation. Nevertheless, this shortcoming can be eliminated by integrating QDs with dyes that have circular polarized emission.[144] One more alternative remedy is to adopt well-aligned quantum rods.[145] Such method might as well facilitate a way to attain greater color separation efficiency in LCD compared to the conventional color filter matrix by improving the quantum yield of QDs. In addition, the compatibility of QDs has also recently demonstrated by Goossens et al. when they developed a broadband image sensor array made of CMOS graphene-QDs.[146]

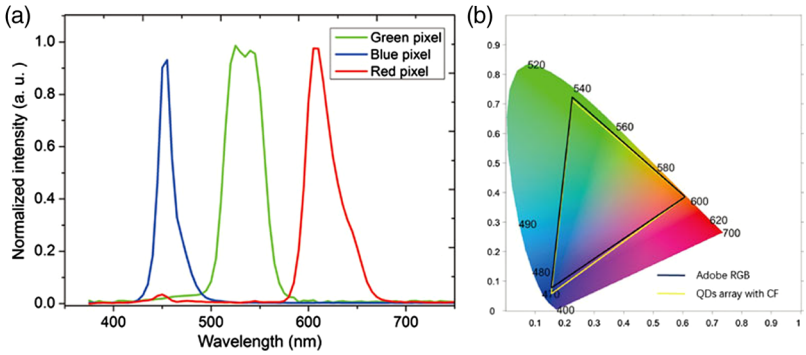

Fig. 20 (a). Filter performance showing very low crosstalk exhibited by a quantum dot filter and (b) comparison of Adobe RGB to color gamut of a quantum dot filter with enhanced active color filter array. Images are from Ref. 139.

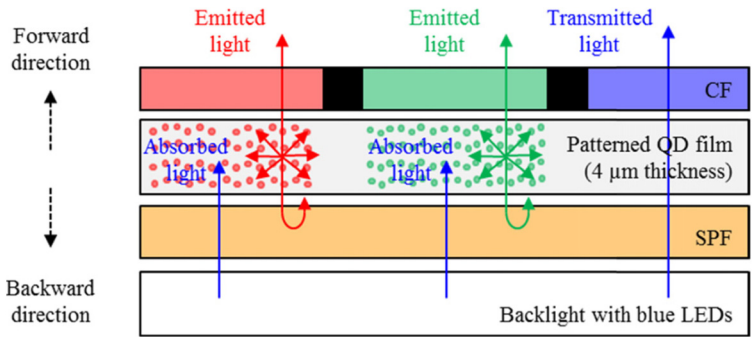

Fig. 21 Schematic diagram of the QD filter proposed in Ref. 142.

7 Conclusion

In this paper, we have reviewed various kinds of nanostructure color filters. Compared to the traditional color filters, the nanostructure color filters can offer some new characteristics including but not limited to minuscule dimensions, enhanced durability, extensive color tunability, and high manufacturing efficiency. With these characteristics, nanostructure color filters may replace the traditional color filters in CMOS digital cameras and find a wide range of novel applications in artificial camouflage, optical data storage, and others. Depending on the color filtering principle, each of these nanostructures possesses a different set of strengths and weaknesses that may suit different kinds of applications.

To make a comparison between these nanostructure color filters, we present a table highlighting their performance in different aspects. Every nanostructure color filtering technology is analyzed in the following five figures of merits we covered earlier: color clarity, spatial resolution, polarization independence, dynamic tuning, and manufacturability. These qualities were chosen because they are critical for the consideration to adopt a suitable nanostructure for certain application. It is easy to see from Table 1 that each method has their own strength and weakness. For example, quantum dot filters are pretty good with their color clarity, but they do not support dynamic tuning. On the other hand, nanowire filters are behind in terms of color vibrancy but provide excellent simplicity in fabrication and they do not require additional filter or polarizer (in case of applications involving polarization). We may overcome this trade-off and maximizing potential of each filter while playing down their weakness by implementing the right structure for the desired application.

Based on Table 1, we can see that plasmonic-based structures are the most promising and mature technology in the near future. This is due to their high performance in most of the filtering aspects. They have high spatial resolution beyond the diffraction limit while at the same time only requiring simple fabrication processes that are highly scalable. Plasmonic-based filters also excel in applications requiring polarization independency, thanks to their localized plasmon resonances, which has low angle-dependent scattering properties. However, plasmonic filters are still lagging behind other nanostructures in terms of color clarity. There are several factors affecting this low performance, for instance, due to the intrinsic losses in metals used in the nanostructure, which contributes to poor Q-factor. This issue can be addressed using low-loss Al-doped Ag materials and taking advantage of hybridization and Fano resonances.[148] In addition, there are also some drawbacks from other nanostructures, some are relatively easy to be improved some are quite difficult to mitigate. For example, many metamaterial filters are also depending on diffractive structure in order to produce vivid colors. This affects the angle dependency of the filter and consequently affects the viewing independence. However, this can be overcome by utilizing a symmetrical pattern on the surface at the cost of losing the tunability of the filter. Additionally, there are also several other qualities worth mentioned apart from those elaborated above such as durability and compatibility. The resilience toward abrasion and bleaching, known as the durability, is also crucial for any coloring method. Traditional filters made of pigments and dyes are susceptible to heat and ultraviolet radiation due to their relatively low chemical stability, often resulting in degradation in filtering performances while nanostructure filters are more robust, and its color quality can be protected from external factors such as longtime sunlight exposure with adequate coatings. Compatibility determines how easy it is to integrate

Table 1 Comparison of various filtering methods.

Structure	Pigments and dyes	Plasmonic	Nanowire	Metamaterial	Quantum dots
Color clarity	High transmissions made it possible to realize bright colors	Low, there is a trade-off between color brightness and saturation	Color correction is sometimes needed but there is no need of external filters	High color purity and wide color gamut	Very bright color, low crosstalk, able to realize 98% adobe color gamut
Spatial resolution	Very low, about 10 m	100,000 dots per inch (DPI), ~diffraction limit	Limited to the NW radii	Extremely high (100,000) DPI has been demonstrated for metal and around 25,000 for all dielectric structure	Each pixel responsible for the color filtering is very tiny. The size of individual quantum dot is smaller than Bohr radius of the material
Polarization sensitivity	Insensitive	Structures with symmetry can be made insensitive. Some grating and broken-symmetry structures are highly sensitive to oblique incidence	Generally insensitive but polarization resolved imaging has also been proposed	Similar to plasmonics, symmetrical structures are in general insensitive. Asymmetric ones can utilize its polarization sensitivity as the filtering mechanism	Sensitive, but polarization loss can be mitigated using dyes that have circular polarized emission
Dynamic tuning	Not possible	Can be done using polarization and electro-optic effect to alter effective index of the structure	Not possible	Possibilities have shown using methods such as electrodeposition, chemical or polarization sensitive structures	Not possible
Manufacturability	Requires multistep processing to integrate the pixels together for realizing colourful images	Can be easily fabricated even with just a few lithography steps	Very practical, since all filter structures can be made simultaneously using one lithography step	Mass production problem since EBL-base approaches are not relevant for industry due to very costly investment and operation as well as low throughput. Polymer replication approach might be used as the solution[147]	Needs a well-controlled nanotransfer process to produce uniform film and smooth surface morphology. But very cost-effective and scalable
Applications	CMOS image sensors, display technology	Cryptography, optical data archival, light emission modification, harmonic generation, plasmonic lasing, photoluminescence enhancement	Filter-less imager, energy harvester, holographic display, wideband multispectral imaging	Surface-enhanced Raman scattering, optical camouflage, biomedical diagnostics	High-resolution display, LED

the filter with another structure or material. This is crucial to make the technology industrially feasible. To conclude, the overall outlook for improved nanostructure color filters and widespread industry adoption remain positive as the development of advanced materials and fabrication technologies will keep on evolving in the years to come.

Disclosures

The authors declare no conflict of interest.

Acknowledgments

The work is financially supported by National Natural Science Foundation of China (NSFC) with the Award no. 61874072.

References

1. H.-S. Koo, M. Chen, and P.-C. Pan, "LCD-based color filter films fabricated by a pigment-based colorant photo resist inks and printing technology," *Thin Solid Films* **515**(3), 896–901 (2006).
2. M. C. Gather et al., "Solution-processed full-color polymer organic light-emitting diode displays fabricated by direct photolithography," *Adv. Funct. Mater.* **17**(2), 191–200 (2007).
3. H. Ghiradella, "Light and color on the wing: structural colors in butterflies and moths," *Appl. Opt.* **30**(24), 3492–3500 (1991).
4. C. Gower, "The cause of blue color as found in the bluebird (sialia sialis) and the blue jay (cyanocitta cristata)," *Auk Ornithol. Adv.* **53**(2), 178–185 (1936).
5. C. L. Ralph, "The control of color in birds," *Am. Zool.* **9**(2), 521–530 (1969).
6. R. M. Strong, "The development of color in the definitive feather," *Science* **15**(379), 527–527 (1902).
7. P. Vukusic et al., "Sculpted-multilayer optical effects in two species of papilio butterfly," *Appl. Opt.* **40**(7), 1116–1125 (2001).
8. S. Wright, "Color inheritance in mammals results of experimental breeding can be linked up with chemical researches on pigments—coat colors of all mammals classified as due to variations in action of two enzymes," *J. Heredity* **8**(5), 224–235 (1917).
9. M. Burresi et al., "Bright-white beetle scales optimize multiple scattering of light," *Sci. Rep.* **4**, 6075 (2014).
10. S. Kinoshita and S. Yoshioka, "Structural colors in nature: the role of regularity and irregularity in the structure," *ChemPhysChem* **6**(8), 1442–1459 (2005).
11. A. R. Parker, "515 million years of structural colour," *J. Opt. A Pure Appl. Opt.* **2**(6), R15 (2000).
12. P. Sciau, *Nanoparticles in Ancient Materials: The Metallic Lustre Decorations of Medieval Ceramics*, INTECH Open Access Publisher, London, Vol. **115** (2012).
13. J. Xu et al., "Wavelength-converted/selective waveguiding based on composition-graded semiconductor nanowires," *Nano Lett.* **12**(9), 5003–5007 (2012).
14. J. Walia et al., "Color generation and refractive index sensing using diffraction from 2-D silicon nanowire arrays," *Small* **10**(1), 143–143 (2014).
15. W. Yue et al., "Highly reflective subtractive color filters capitalizing on a silicon metasurface integrated with nanostructured aluminum mirrors," *Laser Photonics Rev.* **11**(3), 1600285 (2017).
16. Y. Kang et al., "Quantum dots for wide color gamut displays from photoluminescence to electroluminescence," *Nanoscale Res. Lett.* **12**(1), 154 (2017).
17. H. E. Hinton and D. F. Gibbs, "An electron microscope study of the diffraction gratings of some carabid beetles," *J. Insect Physiol.* **15**(6), 959–962 (1969).
18. X. Jiang et al., "Fabrication of coaxial plasmonic crystals by focused ion beam milling and electron-beam lithography," *Mater. Lett.* **100**, 192–194 (2013).

19. J. T. Lv et al., "Plasmonic nanoantennae fabricated by focused ion beam milling," *Int. J. Precis. Eng. Manuf.* **16**(4), 851–855 (2015).
20. G. Si et al., "Direct and accurate patterning of plasmonic nanostructures with ultrasmall gaps," *Nanoscale* **5**(10), 4309–4313 (2013).
21. T. Atay, J.-H. Song, and A. V. Nurmikko, "Strongly interacting plasmon nanoparticle pairs: from dipole–dipole interaction to conductively coupled regime," *Nano Lett.* **4**(9), 1627–1631 (2004).
22. W. Huang et al., "The effect of plasmon field on the coherent lattice phonon oscillation in electron-beam fabricated gold nanoparticle pairs," *Nano Lett.* **7**(10), 3227–3234 (2007).
23. B. Ai et al., "Responsive monochromatic color display based on nanovolcano arrays," *Adv. Opt. Mater.* **1**(10), 679–679 (2013).
24. A. R. Parker, "Natural photonic engineers," *Mater. Today* **5**(9), 26–31 (2002).
25. Y. Zhao et al., "Bio-inspired variable structural color materials," *Chem. Soc. Rev.* **41**(8), 3297–3317 (2012).
26. A. Wang and Y. Dan, "Mid-infrared plasmonic multispectral filters," *Sci. Rep.* **8**(1), 11257 (2018).
27. W. L. Barnes, A. Dereux, and T. W. Ebbesen, "Surface plasmon subwavelength optics," *Nature* **424**(6950), 824–830 (2003).
28. C. Genet and T. W. Ebbesen, "Light in tiny holes," *Nature* **445**(7123), 39–46 (2007).
29. H. A. Atwater, "The promise of plasmonics," *Sci. Am.* **296**(4), 56–62 (2007).
30. J. Li et al., "Photonic crystal formed by the imaginary part of the refractive index," *Adv. Mater.* **22**(24), 2676–2679 (2010).
31. S. A. Maier and H. A. Atwater, "Plasmonics: localization and guiding of electromagnetic energy in metal/dielectric structures," *J. Appl. Phys.* **98**(1), 011101 (2005).
32. Y. Gao et al., "Single-mode graphene-coated nanowire plasmonic waveguide," *Opt. Lett.* **39**(20), 5909–5912 (2014).
33. M.-M. Jiang et al., "Tunability of hybridized plasmonic waveguide mediated by surface plasmon polaritons," *Phys. Chem. Chem. Phys.* **16**(30), 16233–16240 (2014).
34. H. E. Arabi et al., "A high throughput supra-wavelength plasmonic bull's eye photon sorter spatially and spectrally multiplexed on silica optical fiber facet," *Opt. Express* **21**(23), 28083–28094 (2013).
35. J. Le Perchec et al., "Subwavelength optical absorber with an integrated photon sorter," *Appl. Phys. Lett.* **100**(11), 113305 (2012).
36. W. Li et al., "Refractory plasmonics with titanium nitride: broadband metamaterial absorber," *Adv. Mater.* **26**(47), 7959–7965 (2014).
37. X. Xiong et al., "Structured metal film as a perfect absorber," *Adv. Mater.* **25**(29), 3994–4000 (2013).
38. P. Jia et al., "Plasmonic nanohole array sensors fabricated by template transfer with improved optical performance," *Nanotechnology* **24**(19), 195501 (2013).
39. E. Kazuma and T. Tatsuma, "Localized surface plasmon resonance sensors based on wavelength-tunable spectral dips," *Nanoscale* **6**(4), 2397–2405 (2014).
40. S. Papaioannou et al., "Active plasmonics in WDM traffic switching applications," *Sci. Rep.* **2**, 652 (2012).
41. Z. Fang and X. Zhu, "Plasmonics in nanostructures," *Adv. Mater.* **25**(28), 3840–3856 (2013).
42. J. Lv et al., "Plasmon-enhanced sensing: current status and prospects," *J. Nanomater.* **2015**, 1–10 (2015).
43. Y. Yu et al., "Transmissive/reflective structural color filters: theory and applications," *J. Nanomater.* **2014**, 1–17 (2014).
44. T. W. Ebbesen et al., "Extraordinary optical transmission through sub-wavelength hole arrays," *Nature* **391**(6668), 667–669 (1998).
45. S. Yokogawa, S. P. Burgos, and H. A. Atwater, "Plasmonic color filters for CMOS image sensor applications," *Nano Lett.* **12**(8), 4349–4354 (2012).
46. G. Si et al., "Annular aperture array based color filter," *Appl. Phys. Lett.* **99**(3), 033105 (2011).
47. L. Tang, S. Latif, and D. A. B. Miller, "Plasmonic device in silicon CMOS," *Electron. Lett.* **45**(13), 706–708 (2009).

48. E. Balaur et al., "Continuously tunable, polarization controlled, colour palette produced from nanoscale plasmonic pixels," *Sci. Rep.* **6**, 28062 (2016).
49. Q. Chen et al., "CMOS photodetectors integrated with plasmonic color filters," *IEEE Photonics Technol. Lett.* **24**(3), 197–199 (2012).
50. X. Hu, L. Zhan, and Y. Xia, "Color filters based on enhanced optical transmission of sub-wavelength-structured metallic film for multicolor organic light-emitting diode display," *Appl. Opt.* **47**(23), 4275–4279 (2008).
51. C. Liu, V. Kamaev, and Z. V. Vardeny, "Efficiency enhancement of an organic light-emitting diode with a cathode forming two-dimensional periodic hole array," *Appl. Phys. Lett.* **86**(14), 143501 (2005).
52. Y. Qiu et al., "Demonstration of color filters for OLED display based on extraordinary optical transmission through periodic hole array on metallic film," *Displays* **32**(5), 308–312 (2011).
53. Y. Horie et al., "Visible wavelength color filters using dielectric subwavelength gratings for backside-illuminated CMOS image sensor technologies," *Nano Lett.* **17**(5), 3159–3164 (2017).
54. D. V. Labeke et al., "An angle-independent frequency selective surface in the optical range," *Opt. Express* **14**(25), 11945–11951 (2006).
55. M. F. Fouladi, A. Mokhtari, and M. Mehran, "Dual mode operation, highly selective nanohole array-based plasmonic colour filters," *Nanotechnology* **28**(38), 385203 (2017).
56. Y. Yu et al., "Spatial optical crosstalk in CMOS image sensors integrated with plasmonic color filters," *Opt. Express* **23**(17), 21994–22003 (2015).
57. R. W. Wood, XLII, "On a remarkable case of uneven distribution of light in a diffraction grating spectrum," *Philos. Mag. Ser.* **4**(21), 396–402 (2009).
58. K. Knop, "Diffraction gratings for color filtering in the zero diffraction order," *Appl. Opt.* **17**(22), 3598–3603 (1978).
59. K. Knop, "Rigorous diffraction theory for transmission phase gratings with deep rectangular grooves," *J. Opt. Soc. Am.* **68**(9), 1206–1210 (1978).
60. Y. Kanamori, M. Shimono, and K. Hane, "Fabrication of transmission color filters using silicon subwavelength gratings on quartz substrates," *IEEE Photonics Technol. Lett.* **18**(20), 2126–2128 (2006).
61. N. Ganesh et al., "Compact wavelength detection system incorporating a guided-mode resonance filter," *Appl. Phys. Lett.* **90**(8), 081103 (2007).
62. P. B. Catrysse et al., "One-mode model for patterned metal layers inside integrated color pixels," *Opt. Lett.* **29**(9), 974–976 (2004).
63. H.-S. Lee et al., "Color filter based on a subwavelength paterned metal grating," *Opt. Express* **15**(23), 15457–15463 (2007).
64. Y. Ye et al., "Color filter based on a submicrometer cascaded grating," *Opt. Commun.* **283**(4), 613–616 (2010).
65. Z.-C. Ye et al., "Compact transreflective color filters and polarizers by bilayer metallic nanowire gratings on flexible substrates," *IEEE J. Sel. Topics Quantum Electron.* **19**(3), 4800205 (2013).
66. Y. Liang et al., "Extraordinary optical properties in the subwavelength metallodielectric free-standing grating," *Opt. Express* **22**(16), 19484–19494 (2014).
67. L. J. Guo et al., "Ultrathin nanogratings enable high-resolution spectral filtering and imaging," *SPIE Newsroom* (2011).
68. Y. T. Yoon, C. H. Park, and S. S. Lee, "Highly efficient color filter incorporating a thin metal-dielectric resonant structure," *Appl. Phys. Express* **5**(2), 022501 (2012).
69. C. H. Park, Y. T. Yoon, and S. S. Lee, "Polarization-independent visible wavelength filter incorporating a symmetric metal-dielectric resonant structure," *Opt. Express* **20**(21), 23769–23777 (2012).
70. J. Zheng, Z. M. Sheng, and Z. C. Ye, "Reflective low-sideband plasmonic structural colors," *Opt. Mater. Express* **6**(2), 381–387 (2016).
71. J. Wang et al., "Ultra-thin plasmonic color filters incorporating free-standing resonant membrane waveguides with high transmission efficiency," *Appl. Phys. Lett.* **110**(3), 031110 (2017).

72. H. Nishihara, M. Haruna, and T. Suhara, *Optical Integrated Circuits*, McGraw Hill, New York (1989).
73. V. R. Shrestha et al., "Polarization-tuned dynamic color filters incorporating a dielectric-loaded aluminum nanowire array," *Sci. Rep.* **5**, 12450 (2015).
74. M. Taghinejad et al., "Sharp and tunable crystal/Fano-type resonances enabled by out-of-plane dipolar coupling in plasmonicnanopatch arrays," *Ann. Phys.* **530**(10), 1700395 (2018).
75. W. Zhou et al., "Delocalized lattice plasmon resonances show dispersive quality factors," *J. Phys. Chem. Lett.* **3**(10), 1381–1385 (2012).
76. W. Zhou and T. W. Odom, "Tunable subradiant lattice plasmons by out-of-plane dipolar interactions," *Nat. Nanotechnol.* **6**(7), 423–427 (2011).
77. Y. Hua, A. K. Fumani, and T. W. Odom, "Tunable lattice plasmon resonances in 1D nanogratings," *ACS Photonics* **6**(2), 322–326 (2019).
78. M. J. Huttunen et al., "Ultra-strong polarization dependence of surface lattice resonances with out-of-plane plasmon oscillations," *Opt. Express* **24**(25), 28279–28289 (2016).
79. G. H. Y. Li and G. Li, "Necessary conditions for out-of-plane lattice plasmons in nanoparticle arrays," *J. Opt. Soc. Am. B* **36**(4), 805–810 (2019).
80. B. Zeng, Y. Gao, and F. J. Bartoli, "Ultrathin nanostructured metals for highly transmissive plasmonic subtractive color filters," in *Conf. Lasers and Electro-Opt. (CLEO)*, IEEE, pp. 1–2 (2014).
81. X. L. Hu et al., "Influence of film thickness and nanograting period on color-filter behaviors of plasmonic metal Ag films," *J. Appl. Phys.* **115**(11), 113104 (2014).
82. Y. K. Wu et al., "Angle-insensitive structural colours based on metallic nanocavities and coloured pixels beyond the diffraction limit," *Sci. Rep.* **3**(6119), 1194 (2013).
83. K. Kumar et al., "Printing colour at the optical diffraction limit," *Nat. Nanotechnol.* **7**(9), 557–561 (2012).
84. T. Xu et al., "Plasmonic nanoresonators for high-resolution colour filtering and spectral imaging," *Nat. Commun.* **1**, 59 (2010).
85. J. J. Wang et al., "High-performance nanowire-grid polarizers," *Opt. Lett.* **30**(2), 195–197 (2005).
86. X. Jiang et al., "Tuning plasmon resonance in depth-variant plasmonic nanostructures," *Mater. Des.* **96**, 64–67 (2016).
87. V. R. Shrestha et al., "Aluminum plasmonics based highly transmissive polarization-independent subtractive color filters exploiting a nanopatch array," *Nano Lett.* **14**(11), 6672–6678 (2014).
88. G. Si et al., "Reflective plasmonic color filters based on lithographically patterned silver nanorod arrays," *Nanoscale* **5**(14), 6243–6248 (2013).
89. L. K. van Vugt et al., "Size-dependent waveguide dispersion in nanowire optical cavities: slowed light and dispersionless guiding," *Nano Lett.* **9**(4), 1684–1688 (2009).
90. Y. Chen et al., "Compact optical short-pass filters based on microfibers," *Opt. Lett.* **33**(21), 2565–2567 (2008).
91. X. Jiang et al., "Integrated Raman spectroscopic sensor based on silicon nanowire waveguides," *Proc. SPIE* **9274**, 92740I (2014).
92. Y. Ding et al., "Nanowires/microfiber hybrid structure multicolor laser," *Opt. Express* **17**(24), 21813–21818 (2009).
93. M. Khorasaninejad and S. S. Saini, "Silicon nanowire optical waveguide (snow)," *Opt. Express* **18**(22), 23442–23457 (2010).
94. J. Xu et al., "Room-temperature dual-wavelength lasing from single-nanoribbon lateral heterostructures," *J. Am. Chem. Soc.* **134**(30), 12394–12397 (2012).
95. B. Piccione et al., "All-optical active switching in individual semiconductor nanowires," *Nat. Nanotechnol.* **7**(10), 640–645 (2012).
96. L. Cao et al., "Tuning the color of silicon nanostructures," *Nano Lett.* **10**(7), 2649–2654 (2010).
97. L. Cao et al., "Resonant germanium nanoantenna photodetectors," *Nano Lett.* **10**(4), 1229–1233 (2010).

98. A. W. Snyder and J. Love, *Optical Waveguide Theory*, Springer Science & Business Media, New York (2012).
99. L. Cao et al., "Engineering light absorption in semiconductor nanowire devices," *Nat. Mater.* **8**(8), 643–647 (2009).
100. A. Solanki et al., "Geometrical control of photocurrent in active Si nanowire devices," *Nano Energy* **1**(5), 714–722 (2012).
101. S.-K. Kim et al., "Tuning light absorption in core/shell silicon nanowire photovoltaic devices through morphological design," *Nano Lett.* **12**(9), 4971–4976 (2012).
102. H. Park and K. B. Crozier, "Multispectral imaging with vertical silicon nanowires," *Sci. Rep.* **3**, 2460 (2013).
103. H. Park, K. Seo, and K. B. Crozier, "Polymer-embedded arrays of vertical silicon nanowires as color filters," in *CLEO: Sci. and Innovations*, Optical Society of America, p. CM3M–5 (2012).
104. K. B. Crozier et al., "Controlling the light absorption in a photodetector via nanowire waveguide resonances for multispectral and color imaging," *IEEE J. Sel. Topics Quantum Electron.* **24**(6), 1–12 (2018).
105. J. Ye et al., "Optical wavelength filters based on photonic confinement in semiconductor nanowire homojunctions," *Adv. Mater.* **26**(4), 620–624 (2014).
106. K. Seo et al., "Multicolored vertical silicon nanowires," *Nano Lett.* **11**(4), 1851–1856 (2011).
107. H. Park et al., "Filter-free image sensor pixels comprising silicon nanowires with selective color absorption," *Nano Lett.* **14**(4), 1804–1809 (2014).
108. J. S. Yoon et al., "Optical characteristics of silicon-based asymmetric vertical nanowire photodetectors," *IEEE Trans. Electron Devices* **64**(5), 2261–2266 (2017).
109. H. Park and K. B. Crozier, "Elliptical silicon nanowire photodetectors for polarization-resolved imaging," *Opt. Express* **23**(6), 7209–7216 (2015).
110. C. M. Soukoulis and M. Wegener, "Past achievements and future challenges in the development of three-dimensional photonic metamaterials," *Nat. Photonics* **5**(9), 523–530 (2011).
111. D. R. Smith et al., "Determination of effective permittivity and permeability of metamaterials from reflection and transmission coefficients," *Phys. Rev. B* **65**(19), 195104 (2002).
112. V. G. Veselago, "The electrodynamics of substances with simultaneously negative values of ? and μ," *Soviet Phys. Uspekhi* **10**(4), 509–514 (1968).
113. M. K. Hedayati and M. Elbahri, "Review of metasurface plasmonic structural color," *Plasmonics* **12**(5), 1463–1479 (2017).
114. K. Yao and Y. Liu, "Plasmonic metamaterials," *Nanotechnol. Rev.* **3**(2), 177–210 (2014).
115. A. V. Kildishev, A. Boltasseva, and V. M. Shalaev, "Planar photonics with metasurfaces," *Science* **339**(6125), 1232009 (2013).
116. W. Yue et al., "Subtractive color filters based on a silicon-aluminum hybrid-nanodisk metasurface enabling enhanced color purity," *Sci. Rep.* **6**, 29756 (2016).
117. D. Rosenmann et al., "Realizing structural color generation with aluminum plasmonic V-groove metasurfaces," *Opt. Express* **25**(17), 20454–20465 (2017).
118. G. Wang et al., "Mechanical chameleon through dynamic real-time plasmonic tuning," *ACS Nano* **10**(2), 1788–1794 (2016).
119. S. Sun et al., "Real-time tunable colors from microfluidic reconfigurable all-dielectric metasurfaces," *ACS Nano* **12**(3), 2151–2159 (2018).
120. D. Franklin et al., "Polarization-independent actively tunable colour generation on imprinted plasmonic surfaces," *Nat. Commun.* **6**, 7337 (2015).
121. A. Boltasseva and H. A. Atwater, "Low-loss plasmonic metamaterials," *Science* **331**(6015), 290–291 (2011).
122. P. R. West et al., "Searching for better plasmonic materials," *Laser Photonics Rev.* **4**(6), 795–808 (2010).
123. J. V. D. Groep and A. Polman, "Designing dielectric resonators on substrates: combining magnetic and electric resonances," *Opt. Express* **21**(22), 26285–26302 (2013).

124. J. Proust et al., "All-dielectric colored metasurfaces with silicon Mie resonators," *ACS Nano* **10**(8), 7761–7767 (2016).
125. V. Vashistha et al., "All-dielectric metasurfaces based on cross-shaped resonators for color pixels with extended gamut," *ACS Photonics* **4**(5), 1076–1082 (2017).
126. Y. Yi et al., "Strong visible magnetic resonance of size-controlled silicon-nanoblock metasurfaces," *Appl. Phys. Express* **9**(4), 042001 (2016).
127. Y. F. Yu et al., "High-transmission dielectric metasurface with 2 phase control at visible wavelengths," *Laser Photonics Rev.* **9**(4), 412–418 (2015).
128. I. Staude et al., "Tailoring directional scattering through magnetic and electric resonances in subwavelength silicon nanodisks," *ACS Nano* **7**(9), 7824–7832 (2013).
129. A. I. Kuznetsov et al., "Magnetic light," *Sci. Rep.* **2**(7), 492 (2012).
130. C. S. Park et al., "Structural color filters enabled by a dielectric metasurface incorporating hydrogenated amorphous silicon nanodisks," *Sci. Rep.* **7**(1), 2556 (2017).
131. V. Vashistha et al., "Polarization tunable all-dielectric color filters based on cross-shaped Si nanoantennas," *Sci. Rep.* **7**(1), 8092 (2017).
132. B. Yang et al., "Polarization-sensitive structural colors with hue-and-saturation tuning based on all-dielectric nanopixels," *Adv. Opt. Mater.* **6**(4), 1701009 (2018).
133. L. Kim et al., "Contact printing of quantum dot light-emitting devices," *Nano Lett.* **8**(12), 4513–4517 (2008).
134. J. Bao and M. G. Bawendi, "A colloidal quantum dot spectrometer," *Sci. Found. China* **523**(7558), 67–70 (2015).
135. T. H. Kim et al., "Full-colour quantum dot displays fabricated by transfer printing," *Nat. Photonics* **5**(3), 176–182 (2011).
136. N. Dhindsa and S. S. Saini, "Localized absorption in aluminum mask in visible spectrum due to longitudinal modes in vertical silicon nanowire arrays," *J. Appl. Phys.* **117**(22), 224302 (2015).
137. L. Zhang, "Quantum dot color filter, liquid crystal panel and display device," CN 102944943 A (2013).
138. H. Chen, J. He, and S. T. Wu, "Recent advances on quantum-dot-enhanced liquid crystal displays," *IEEE J. Sel. Topics Quantum Electron.* **23**(5), 1–1 (2017).
139. Y. Liu et al., "A quantum dot array for enhanced tricolor liquid-crystal display," *IEEE Photonics J.* **9**(1), 1–7 (2017).
140. H.-J. Kim et al., "61-2: optical efficiency enhancement in wide color gamut LCD by a patterned quantum dot film and short pass reflector," in *SID Symp. Digest of Tech. Papers*, Wiley Online Library, Vol. 47, pp. 827–829 (2016).
141. G. Kim, Y. C. Shih, and F. Shi, "Optimal design of quantum dot color conversion film in LCD backlighting," *IEEE J. Sel. Topics Quantum Electron.* **23**(99), 1–4 (2017).
142. H. J. Kim et al., "Realization of 95% of the Rec. 2020 color gamut in a highly efficient LCD using a patterned quantum dot film," *Opt. Express* **25**(10), 10724–10734 (2017).
143. R. Butté et al., "Recent progress in the growth of highly reflective nitride-based distributed Bragg reflectors and their use in microcavities," *Jpn. J. Appl. Phys.* **44**(10), 7207–7216 (2005).
144. D. Zhao et al., "Light-emitting liquid crystal displays based on an aggregation-induced emission luminogen," *Adv. Opt. Mater.* **3**(2), 199–202 (2015).
145. M. Hasegawa and Y. Hirayama, "Use of quantum rods for display applications," *J. Soc. Inf. Disp.* **24**(5), 286–292 (2016).
146. S. Goossens et al., "Broadband image sensor array based on graphene–CMOS integration," *Nat. Photonics* **11**(6), 366–371 (2017).
147. E. Højlund-Nielsen et al., "Plasmonic colors: toward mass production of metasurfaces," *Adv. Mater. Technol.* **1**(7), 1600054 (2016).
148. C. Zhang et al., "High-performance doped silver films: overcoming fundamental material limits for nanophotonic applications," *Adv. Mater.* **29**(19), 1605177 (2017).

Felix Gildas received his BEng degree in electronic information engineering from Beijing University of Aeronautics and Astronautics, Beijing, 2016 and his MSc degree in electrical and

computer engineering (ECE) from the University of Michigan–Shanghai Jiao Tong University Joint Institute (UM-SJTU JI), Shanghai Jiao Tong University in 2019.

Yaping Dan is an associate professor of electrical engineering at the University of Michigan–Shanghai Jiao Tong University Joint Institute (UM-SJTU JI), Shanghai Jiao Tong University in Shanghai. He received his bachelor's degree in electrical engineering from Xi'an Jiaotong University, Xi'an in 1999 and his master's degree in microelectronics from Tsinghua University, Beijing in 2002, and PhD in electrical engineering from the University of Pennsylvania, US in 2008. Before he joined the Joint Institute, he was a postdoctoral fellow and then research associate at Harvard University.